752 *Macromolecules* **2010**, *43*, 752–764
DOI: 10.1021/ma9020533

Macromolecules
ARTICLE

Soap-Free Emulsion Polymerization of Poly(ethylene glycol)-*block*-poly(*N*-isopropylacrylamide): Elucidation of Specific Reaction Fields for Quasi-Living Polymerization by Time-Resolved SANS

Ryuhei Motokawa,[†] **Satoshi Koizumi,**[*,†] **Takeji Hashimoto,**[†] **Masahiko Annaka,**[‡] **and Takayuki Nakahira**[§]

[†]*Advanced Science Research Center, Japan Atomic Energy Agency, Ibaraki 319-1195, Japan,* [‡]*Department of Chemistry, Kyushu University, Fukuoka 812-8581, Japan, and* [§]*Department of Applied Chemistry and Biotechnology, Chiba University, Chiba 263-8522, Japan*

Received September 15, 2009; Revised Manuscript Received November 9, 2009

ABSTRACT: Poly(ethylene glycol)-*block*-poly(*N*-isopropylacrylamide) (PEG-*b*-PNIPAAm) was synthesized by radical polymerization of *N*-isopropylacrylamide (NIPAAm) from the radically activated chain ends generated on PEG. The polymerization process was investigated by a conventional observation of molecular weight and its distribution as well as monomer conversion, $C_M(t)$, as a function of the polymerization time t and temperature T_p, by means of time-resolved GPC. The reaction fields in which the polymerization takes place were explored by time-resolved small-angle neutron scattering (SANS). The results elucidated the following characteristics on the temperature-dependence of the solution structure and, hence, the reaction fields: (i) at $15 \le T_p$ (°C) ≤ 30, the solution is composed of swollen micelles in which PNIPAAm and PEG block chains form swollen cores and brushes emanating from the interface between them, respectively; and (ii) at $34 \le T_p$ (°C) ≤ 60, the solution is composed of dehydrated PNIPAAm cores (hard cores) and swollen PEG brushes with well-defined interfaces between them. As for (i) and (ii), the micelles were formed from a very early stage of the polymerization as C_M being as small as 0.05, hence, yielding a "soap-free emulsion polymerization" field for NIPAAm. The results obtained in this work reveal that the hard-core micelle formation is the necessary and sufficient condition for the "quasi-living soap-free emulsion polymerization".

I. Introduction

We have previously reported the synthesis of a block copolymer (bcp) of poly(ethylene glycol)-*block*-poly(*N*-isopropylacrylamide) (PEG-*b*-PNIPAAm) by radical polymerization of (*N*-isopropylacrylamide) (NIPAAm) monomer from the radically activated chain end of monofunctional methoxy-poly(ethylene glycol) (PEG) in an aqueous reaction medium at various polymerization temperatures, T_p, ranging from 25 to 60 °C,[1] following the method reported by Feijen and co-workers.[2] We found that the bcp synthesized at $T_p \ge 34$ °C had the following characteristics of "quasi-living polymerization"[1,2] without using controlled radical polymerization techniques such as atom transfer radical polymerization (ATRP),[3,4] reversible addition−fragmentation chain transfer radical polymerization (RAFT),[5] and nitroxide-mediated living radical polymerization (NMLP):[6] (i) a narrow molecular weight distribution, (ii) a linear relationship between the number-averaged molecular weight M_n and the monomer conversion C_M in the experimentally accessed range of $C_M \ge 0.5$, and (iii) achievement of the final $C_M \ge 0.9$.

In this work, we propose that the origin of the quasi-living polymerization behavior at $T_p \ge 34$ °C is attributable to the formation of dehydrated micelle cores (hard cores) by propagating PNIPAAm block chains, stabilized by brushes of PEG block chains emanating from the cores, from the very early stage of the polymerization and, hence, throughout the course of polymerization. The suppressed mobility of the chain-end radicals, confined inside the cores, make the propagating radicals "long-living" and, hence, the polymerization "quasi-living". The micelles spontaneously formed in the early stage polymerization provide a "reaction field" analogous to that in emulsion polymerization.[7−11] However, the micelles here are formed without incorporation of soaps, so that the polymerization can be coined as "soap-free emulsion polymerization".

Emulsion polymerization is known to provide large molecular weight polymers with a narrow molecular weight distribution as compared to solution polymerization.[12−14] According to electron spin resonance (ESR) measurements, radicals in glassy particles of poly(methyl methacrylate)[12,13] or in solid particles of poly(*N*-methyl acrylamide),[14] live much longer than those in fluid solutions. This is believed to be due to the reduced mobility of chain-end radicals, suppressing bimolecular termination reactions of the radicals and, hence, prolonging their lifetime. The polymerization, which occurs in such particles, is expected to give high molecular weight polymers with a relatively narrow molecular weight distribution.

Feijen and co-workers[2,15] first reported that (a) the radical polymerization of NIPAAm into PEG-*b*-PNIPAAm in an aqueous medium at 50 and 60 °C involves formation of micelles; (b) the polymerization of NIPAAm in the micelles, which they call "in situ emulsion polymerization", exhibits "quasi-living nature", as evidenced not only by a narrow molecular weight distribution, but also by continued polymerization upon addition of monomers after the completion of polymerization.

The phase behavior of the chemically reacting bcp systems as described above, including the micelle formation, is generally described on the basis of statistical mechanics of multicomponent systems composed of A homopolymer, A-B diblock copolymers, and solvent(s), where A and B correspond to PEG and

---

*To whom correspondence should be addressed. Tel.: +81-29-284-3511. Fax: +81-29-282-5939. E-mail: koizumi.satoshi@jaea.go.jp.

PNIPAAm, respectively, and the solvent corresponds to a mixture of water and NIPAAm monomer. Characteristic parameters of such systems are the concentrations of the solvent, A and A-B, degree of polymerizations (DP) of A and B (N_A and N_B, respectively), and thermodynamic interaction parameters between A and B (χ_{AB}), A and S (χ_{AS}), and B and S (χ_{BS}), where N_B increases with time because of the ongoing polymerization. Depending on these parameters, the polymerizing system will exhibit homogeneous solution, the micelle formation,[16,17] ordered microdomains of bcp via order−disorder transition (ODT) and order−order transition (OOT),[18−21] and a macrophase separation between the solvent-rich phase and the polymer-rich phase.[22]

PEG and PNIPAAm block chains exhibit a unique temperature-dependent selective affinity to water due to the LCST-type phase behavior of PNIPAAm in water at $T_{LCST} = 31$ °C,[23−27] whereas PEG is hydrophilic and stable in water over a wide temperature range from far below room temperature to near the boiling point of water. In the range of temperature $T \le 17$ °C, well below T_{LCST} of PNIPAAm in water, the solvent is expected to be neutrally good ($\chi_{AS} \cong \chi_{BS}$).[22,28,29] Under this condition, the solvent equally swells each block chain and screens the segmental interactions between A and B, simply decreasing χ_{AB}.[30−32] Hence, the solution is homogeneous and free from micelle formation.[22]

As the temperature increases, asymmetry between χ_{AS} and χ_{BS} should increase and, hence, the solvent becomes increasingly selective, good for PEG but poor for PNIPAAm. Static small-angle neutron scattering (SANS) and ultrasmall-angle neutron scattering (USANS) measurements on the aqueous solution of neat PEG-*b*-PNIPAAm having the $M_n = 30000$ or less, which was obtained by a purification of the solution after the completion of the polymerization, elucidated that an excess SANS appears above 17 °C due to micelle formation, giving rise to a deviation of the SANS from the Ornstein−Zernicke (OZ) type scattering.[22,28,33] More precisely at $17 \le T$ (°C) ≤ 30, the micelle cores of PNIPAAm block chains are swollen by water ("soft core"), whereas at $T \ge 32$ °C,[22,34] the micelle core is substantially dehydrated and shrunk ("solid-like core" or "hard core"). Consequently, the radical polymerization of NIPAAm to PEG-*b*-PNIPAAm at $T \ge 17$ °C is expected to form micelles in some stage of the polymerization process, so that the polymerization satisfies the necessary condition for the soap-free emulsion polymerization. However, we found that the polymerization in the soft core does not bring about the quasi-living polymerization.[1] Consequently, the necessary and sufficient condition for it appears to be a controlled radical polymerization in the solid-like micellar cores.

In this work, we further employed SANS measurements on the above polymerization system for direct observation of the reaction fields to be developed in the course of NIPAAm polymerization. In the previous SANS and USANS work,[22] the solid-like micellar cores were confirmed only for the solution obtained after the polymerization and purification. In the previous time-resolved GPC work,[1] the living behavior was confirmed only at the later stage of the polymerization process where $C_M(t) \ge 0.5$. By combining in situ and time-resolved SANS and GPC with USANS, we attempted to obtain solid evidence as to the necessary and sufficient condition for the quasi-living behavior of the soap-free emulsion polymerization. Here, we would like to stress that the formation of the solid-like micellar cores in the reaction solution have never been explored so far in situ during the polymerization process. Consequently, a question concerning when the hard-core micelle is formed during the polymerization process is left unexplored, despite the fact that it is crucial for understanding the quasi-living polymerization behaviors. In this work, we wish to address this key question. We would like to stress that the time-resolved SANS gives extremely useful information to address this key question.

II. Experimental Section

II-1. Polymer Synthesis. NIPAAm monomer (Kohjin Co., Fuji, Japan) was purified by a recrystallization from a toluene/*n*-hexane mixture. Monofunctional methoxy-PEG ($M_n = 5 \times 10^3$ and polydispersity index $M_w/M_n = 1.15$, Aldrich) was purified with an activated alumina column using toluene as an eluent. Ceric(IV) ammonium nitrate $Ce(NO_3)_6(NH_4)_2$ (Wako Pure Chemical Co., Osaka, Japan) used as a redox initiator was first dried at 105 °C and then dissolved in 200 mL of 1 N nitric acid to prepare a stock solution of the initiator with 0.1 N.

The polymerization was conducted as follows. PEG, 1.0 g, was dissolved in 10 mL of distilled deionized water in a 100 mL round-bottom flask. To this was added 3.3 mL of the stock solution of the initiator to prepare a solution containing $Ce^{(IV)}$ and PEG with a molar ratio of $[Ce^{(IV)}]/[PEG] = 1.65$. After stirring this solution for 5 min, 0.65 g of NIPAAm dissolved in 10 mL of distilled deionized water was added under the flow of nitrogen gas. The redox initiator produces a radical at the terminal carbon of PEG to start the NIPAAm polymerization. The polymerization was carried out under a positive nitrogen pressure at T_p, ranging from 15 to 60 °C. After the completion of the polymerization, the solution is first dialyzed in water and then precipitated in hot acetone to conduct the GPC measurements on isolated and purified synthesized bcp obtained at the end of the polymerization. The solution undergoing polymerization also was studied by the time-resolved GPC and SANS, as will be described in sections II-2 and II-3, respectively. The initial concentration of NIPAAm monomer, PEG, and $Ce^{(IV)}$ initiator in these reacting systems are 0.25 M, 8.6 mM, and 14.1 mM, respectively.

II-2. Time-Resolved GPC Measurements. We investigated time changes in the amount of PEG, NIPAAm monomer, and the synthesized bcp, PEG-*b*-PNIPAAm, during the course of the polymerization. For this purpose, GPC experiments were performed on so many batches (∼100) of the reaction solutions, which were prepared using the method described in section II-1 and which were terminated at various polymerization times *t* at each T_p. We confirmed reproducibility of the data obtained for different batches at a given set of *t* and T_p.

The difficulties of GPC measurements of PNIPAAm, as reported previously,[35] that is, the possible aggregation of PNIPAAm in the eluent and the adsorption of them to the column packing, were addressed as follows. Each solution at a given set of *t* and T_p was first cooled down in an ice water bath and then diluted by 10 mM $NaNO_3$ aqueous solution to prepare a reaction solution diluted by 1000 times in weight. This process deactivates the chain-end radicals and, hence, brings about the termination reaction. Before running the GPC measurements, the diluted solutions were stored in a refrigerator at 5 °C for at least 24 h to obtain a homogeneous solution containing the bcp. Note that the bcp micelles in the solution, if they existed, are found to be completely dissolved into a homogeneous solution at 10 °C.[22]

The GPC measurements were run at 10 °C with TOSOH HLC-8220 (TOSOH, Tokyo, Japan) with a set of three columns consisting of two $GMPW_{XL}$ columns and one $G2500PW_{XL}$ column having the exclusion limit molecular weight of 5×10^7 and 5×10^3 with dextrane standards in water, respectively. The set of the columns was necessary to identify simultaneously the monomers, the bcps, and PEGs with a sufficient resolution. The flow rate of the eluent used was 1.0 mL/min, and the components in the eluent were monitored with a refractive index detector. We paid special attention to keep the injection volume constant (100 μL) in order to quantitatively evaluate the concentration of each component. The molecular weights of the bcps were calibrated with PEG standards in water.

II-3. In Situ and Time-Resolved SANS and Static USANS. We performed in situ and time-resolved SANS measurements during the course of the polymerization, as well as in situ and static USANS measurements, on the solutions in which

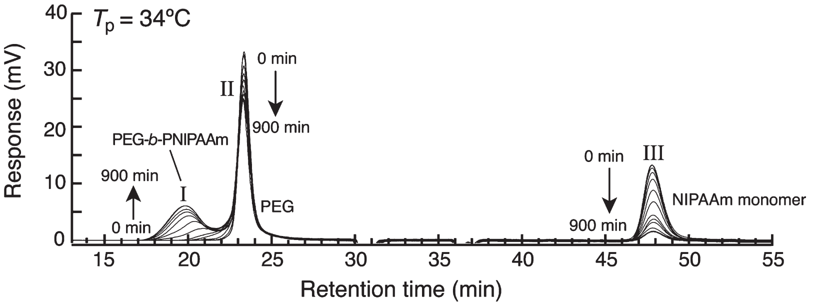

Figure 1. GPC chromatograms obtained in the polymerization process at T_p = 34 °C as a function of time. Peaks I, II, and III are attributed to PEG-*b*-PNIPAAm, PEG, and NIPAAm monomer, respectively.

the polymerization is nearly completed, both with the research reactor JRR3, Japan Atomic Energy Agency (JAEA), at Tokai, Japan, and the SANS and USANS spectrometers installed there. The SANS and USANS experiments were carried out with D_2O solution to gain a sufficient scattering contrast of neutrons between polymers (PEG and bcp) and D_2O. The scattering length densities of PNIPAAm, PEG, and D_2O (defined by b_{PNIPAAm}, b_{PEG}, and $b_{\mathrm{D_2O}}$) are 1.23×10^{-14}, 0.94×10^{-14}, and 9.49×10^{-14} cm^{-2} mol, respectively. The time-resolved SANS measurements at a given T_p were conducted on a given batch of the solution, but those at other T_ps were carried out on different batches of the solutions prepared exactly in the same way. The USANS measurements also were carried out on different batches of the solutions.

The SANS spectrometer (SANS-J) utilizes the pinhole optics,[36,37] while the USANS spectrometer (PNO) utilizes channel-cut single crystals of Si(111) for both in the incident and scattered beam paths.[38-40] Because the resolution of this USANS instrument as observed from the rocking curve is $\Delta q = 4 \times 10^{-4}$ nm^{-1}, structures up to the order of 10 μm can be resolved. SANS-J covers a q range of $3 \times 10^{-2} < q\,(\mathrm{nm}^{-1}) < 2$ by setting the sample-to-detector distance at 10 and 1.5 m and by using the incident neutron beam of wavelength $\lambda = 0.65$ nm and wavelength distribution of $\Delta\lambda/\lambda = 13\%$, where $q\ [\equiv(4\pi/\lambda)\sin(\theta/2)]$ is a magnitude of the scattering vector, with λ and θ being the wavelength of neutrons and the scattering angle.

In the SANS-J, the scattered neutrons were detected by a two-dimensional ^{3}He position-sensitive detector of 0.58 m in diameter and 5 mm resolution. The two-dimensional data were corrected for counting efficiency, instrumental background, and air scattering. After circularly averaging the SANS intensity distribution, we converted the scattering intensity to the absolute intensity unit of cm^{-1} using a secondary standard of an irradiated Al plate. Incoherent scattering from hydrogen, estimated from the incoherent scattering intensity for the reference sample (H_2O), was subtracted from the net absolute intensity. The corrected scattered intensity distribution is designated as $I(q)$ hereafter.

The USANS spectrometer (PNO) with the Bonse-Hart type optics[38] with a triple bounce reflection condition for both a monochromator crystal and an analyzer one ($\lambda = 0.1999$ nm) is capable of covering an ultrasmall-angle q range $[10^{-4} < q\,(\mathrm{nm}^{-1}) < 10^{-2}]$. The scattering profiles with q were corrected for the background scattering and then for the slit-height smearing according to the infinite slit-height approximation.[41] After the corrections, the USANS intensity was converted to the absolute intensity $I(q)$ using the absolute SANS intensity as a calibration standard.

The time-resolved SANS measurement was started immediately after the onset of the polymerization by filling the reaction-started solution into a quartz cell with 2 mm thickness and placing the cell into the incident beam path of neutrons. The dead time brought about for transferring the polymerization-initiated solution into the SANS cell and finally starting the time-resolved SANS experiment is less than 1 min and, hence, is short enough for the present time-resolved studies. Transmission of the reaction system for the SANS was measured only before polymerization, and this value was used for the transmission for all the time-resolved SANS profiles. This correction method is legitimate, because the change in the SANS transmission with time is small, for example, it decreased from 78 to 75% at T_p = 34 °C. The sample temperature was controlled at a given T_p within ±0.1 °C accuracy.

The solution specimens for USANS experiments were prepared with the same recipe as those for SANS. The solutions were filled in a quartz cell with 2 mm thickness and 40 mm in length, and the cell was placed in a temperature enclosure controlled at given T_ps. Prior to the USANS measurement we measured transmittance of the incident neutron beam, $T_r(t)$, during the polymerization process by fixing the analyzing crystal at $q = 0$ nm^{-1} and monitoring the primary beam intensity passing through the sample specimen as a function of t. After $T_r(t)$ reaches a constant steady value, we carried out the USANS measurement. The USANS profiles thus obtained were expected to be the one corresponding to the structures developed in the end of reaction at a given T_p.

III. Results

III-1. Time-Resolved GPC Measurements. Figure 1 represents a typical time evolution of GPC chromatograms obtained at a given T_p = 34 °C. It shows three peaks: peak I and peak II, which are attributed to the polymerized bcp and unreacted PEG, respectively, as well as peak III due to the NIPAAm monomer. As the polymerization proceeds (from 0 to 900 min), peak I moves toward the shorter retention time with increasing intensity, indicating that both chain length and concentration of the bcp increase with t, while peak II and peak III gradually lose their intensities, indicating that the PEG and the monomers are consumed with t.

The value of $C_M(t)$ was determined from the change in the area under peak III with t, that is, $S_M(t)$

$$C_M(t) = 1 - [S_M(t)/S_M(t=0)] \tag{1-a}$$

The consumption of PEG, $C_{\mathrm{PEG}}(t)$, was also evaluated from the change in the area under peak II with t, that is, $S_{\mathrm{PEG}}(t)$

$$C_{\mathrm{PEG}}(t) = 1 - [S_{\mathrm{PEG}}(t)/S_{\mathrm{PEG}}(t=0)] \tag{1-b}$$

At the end of the polymerization, $C_M(t)$ reaches a constant value defined as $C_M(\infty)$ [$C_M(\infty) \sim 0.9$ at T_p = 34 °C], and $C_{\mathrm{PEG}}(t)$ reaches $C_{\mathrm{PEG}}(\infty) \sim 0.25$, which indicates the presence of unreacted PEG in the as-polymerized solution.

Figure 2 highlights the time changes of peaks I and II at T_p ranging from (a) 60 °C to (f) 15 °C. In the early stage of the polymerization, it is difficult to estimate M_n and M_w/M_n of

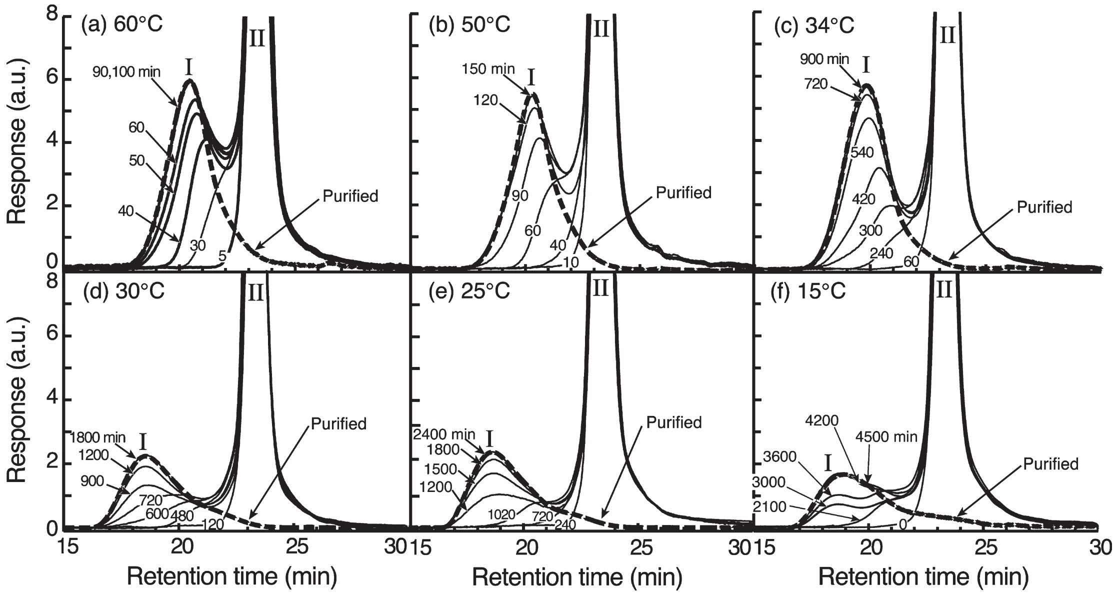

Figure 2. GPC chromatograms obtained at polymerization times (min) and at T_p = (a) 60, (b) 50, (c) 34, (d) 30, (e) 25, and (f) 15 °C, where the chromatograms focused on the retention time between 15 and 30 min. The broken lines show the results obtained with the purified reaction solution after the completion of the reaction and hence elucidate the chromatograms of neat PEG-*b*-PNIPAAm. Each peak for PEG-*b*-PNIPAAm (peak I) at a given time during the polymerization was separated from the peak for PEG (peak II) by assuming a Gaussian profile for PEG-*b*-PNIPAAm.

Table 1. Molecular Characterizations of PEG-*b*-PNIPAAm after the Completion of the Polymerization at Varying T_p[a]

T_p		25	30	34	40	50	60
unpurified	$M_n \times 10^{-4}$	17.0	17.0	11.3	9.5	7.9	7.2
PEG-*b*-PNIPAAm	M_w/M_n	2.17	2.01	1.63	1.60	1.54	1.51
purified	$M_n \times 10^{-4}$	10.6	10.4	11.6	9.4	7.7	7.0
PEG-*b*-PNIPAAm	M_w/M_n	3.27	2.97	1.59	1.55	1.49	1.46
$DP_{PNIPAAm}/DP_{PEG}$		7.8/1	7.6/1	8.5/1	6.9/1	5.5/1	5/1

[a] Number-averaged molecular weights M_n, polydispersity indices M_w/M_n, and ratios of number-average degree of polymerization of PNIPAAm ($DP_{PNIPAAm}$) and PEG block chains (DP_{PEG}) as evaluated by the GPC measurements.

the bcps, because the two peaks overlap each other extensively. However, when $C_M(t)$ exceeds 0.4, we are able to separate the two peaks and to fit peak I reasonably well with a Gaussian function, which enables us to determine $M_n(t)$ and $M_w(t)$ for the bcps. At T_p = 15 °C, peak I is bimodal at $t \geq 3000$ min (see Figure 2f), though its origin is not clear at this moment. Therefore, we shall not evaluate the values of M_n and M_w/M_n at 15 °C as a function of t.

In Figure 2, the chromatograms for the purified samples, shown by broken lines, are free from the unreacted PEG and hence enable us to precisely determine M_n and M_w/M_n of the synthesized bcp at the end of the polymerization. Table 1 shows M_n and M_w/M_n of the bcps evaluated from peak I for the purified and unpurified samples, both after the completion of polymerization. The values M_w/M_n obtained for the purified solution at T_p = 50 and 60 °C are equal to 1.49 and 1.46, respectively, and these values are as small as that of PNIPAAm homopolymers obtained by RAFT or ATRP polymerization.[35,42−44]

At lower T_p's, that is, 25 and 30 °C, M_w/M_n for the purified samples were 3.27 and 2.97, respectively. These values are significantly larger than M_w/M_n (~2.1) evaluated for the unpurified samples. This is because the long tailing of peak I toward the large retention time, which is clearly observed and taken care of for the purified sample, was ignored in the Gaussian approximation of peak I for the unpurified sample. At $T_p \geq 34$ °C, however, we did not find significant differences

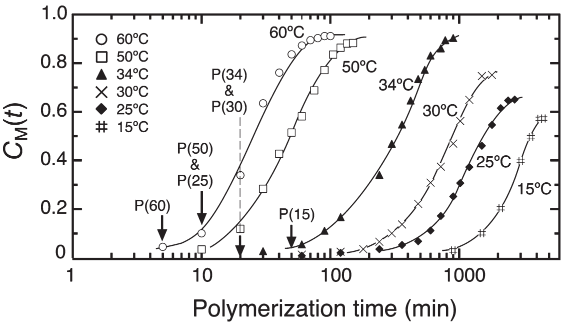

Figure 3. NIPAAm monomer conversion $C_M(t)$ estimated from peak III of the time-resolved GPC chromatograms as a function of polymerization time t and temperature T_p. The solid lines are guides for eyes. The arrow attached to P(T_p), in which P stands for the Porod law, specifies the critical time, t_c, where the hard-core micelle starts to form at T_p = 34, 50, and 60 °C, and the soft-core micelle starts to form at T_p = 15, 25, and 30 °C.

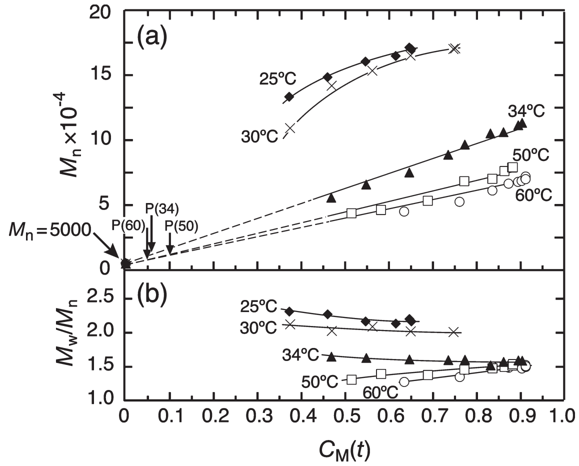

Figure 4. (a) Number-averaged molecular weight M_n and (b) polydispersity index M_w/M_n as a function of NIPAAm monomer conversion $C_M(t)$ at varying T_p. The solid lines and broken lines are guides for eyes. P(T_p) has the same meaning as in Figure 3.

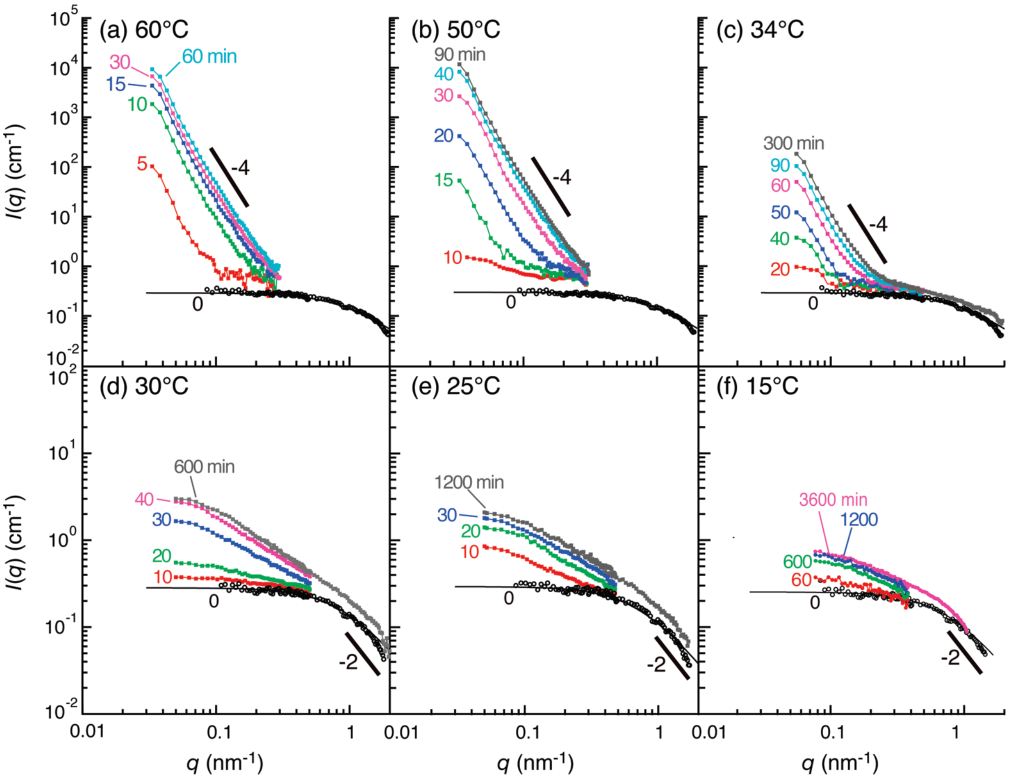

Figure 5. In situ small-angle neutron scattering profiles at varying polymerization time *t* (min) at varying T_p: (a) 60, (b) 50, (c) 34, (d) 30, (e) 25, and (f) 15 °C. The profiles shown by the unfilled circles and the solid lines marked by 0 indicate the experimental and theoretical scattering profiles for the PEG solution prior to the polymerization, respectively, where the theoretical profile was reproduced by the Ornstein−Zernicke theory (eq 2).

in M_w/M_n between the purified and unpurified samples, because the tailing, though existing, contributes less to the entire chromatograms, and hence, the chromatograms for both samples are reproduced by similar Gaussian functions.

The time evolution of $C_M(t)$ at varying T_p is shown in Figure 3. The $C_M(t)$ starts to increase earlier with increasing T_p: for example, at about 5 min at $T_p = 60$ °C and at about 900 min at $T_p = 15$ °C. Note that a large difference of $C_M(\infty)$ is clearly observed between $T_p \geq 34$ °C and $T_p \leq 30$ °C: $C_M(\infty)$ is higher than 0.9 at $T_p \geq 34$ °C and less than 0.75 at $T_p \leq 30$ °C. The arrows labeled with P(T_p) will be explained in section IV-3 later in conjunction with Figures 5 and 8.

M_n and M_w/M_n determined for the unpurified bcps are plotted as a function of $C_M(t)$ at various T_p's from 25 to 60 °C in Figure 4a and b, respectively. We note that M_n and M_w/M_n at a given $C_M(t)$ decrease with T_p, the reason for which will be discussed later in relation to the micelle formation during the course of polymerization. At $T_p \geq 34$ °C, M_n of bcp increases linearly with $C_M(t)$, indicating that the NIPAAm monomers were consumed by polymerization to bcp but not to PNIPAAm homopolymers. This is because the redox initiator produces a radical only at the terminal carbon of a PEG chain, which was confirmed by the fact that no PNIPAAm was formed in the absence of PEG after 12 h at 34 °C. Besides, we clearly recognize the other two signatures (i) and (iii), characteristic of the living-like behaviors of the polymerization, as already described in section I. At lower T_ps, that is, 25 and 30 °C, the living-like behaviors are not discerned at all. M_w/M_n becomes large, ranging between 2.0 and 2.5, and $C_M(t)$ does not increase more than 75% as noted above. The arrows labeled by P(T_p) will be discussed later in section IV-3 in conjunction with Figures 5 and 8.

III-2. In Situ and Time-Resolved SANS. Figure 5 shows time-resolved SANS profiles obtained at various T_ps from (a) 60 °C to (f) 15 °C. For the PEG solution before starting polymerization (t = 0 min), the SANS profiles are well predicted by the Ornstein−Zernicke (OZ) equation,[45] which can be derived by the general RPA equation[46] for polymer solutions for the small q range satisfying $qR_g < 1$,

$$I(q) \sim I(0)/[1+(q\xi)^2] \tag{2}$$

where $I(0)$ and ξ are, respectively, the forward scattering intensity, which depends on the osmotic compressibility of the solution and the correlation length for the thermal concentration fluctuation of PEG in the solution. Both $I(0)$ and ξ depend on polymer concentration ϕ. Because ϕ is finite in our case, we did not use the Debye scattering function for single chains. ξ is related to the radius of gyration R_g of PEG and is calculated in straightforward from the RPA equaton,[46] $\xi^2 = (R_g^{\,2}/3)[(1-\phi+\phi N)/(1-\phi)]^{-1}$ in the case of $\chi = 0$, where χ is the segmental interaction parameter between polymer and solvent and N is the DP of PEG. The solid lines at t = 0 min in Figure 5 were the best-fitted theoretical profiles by using eq 2.

The results shown in Figure 5 reveal themselves that the time evolution of $I(q)$ after the onset of polymerization strongly depends on T_p, that is, $15 \leq T_p$ (°C) ≤ 30, and $T_p \geq 34$ °C. At $T_p \geq 34$ °C, after the initiation of the polymerization, the scattering intensity immediately and rapidly increases with t, showing the q-dependence of $q^{-\beta}$ with β close to 4, that is, the so-called Porod law,[47] elucidating that the PNIPAAm block chains form a micelle core ("hard core") having a well-defined interface in the solution, that is, a smooth interface with a sharp interface boundary. At $15 \leq T_p$ (°C) ≤ 30, on the other hand, the scattering intensity at a given q (e.g., $q \sim 0.08$ nm^{-1}) increases gradually with t and reaches almost a constant value at ∼1200 min, the intensity level of which is at least 2 orders of magnitude

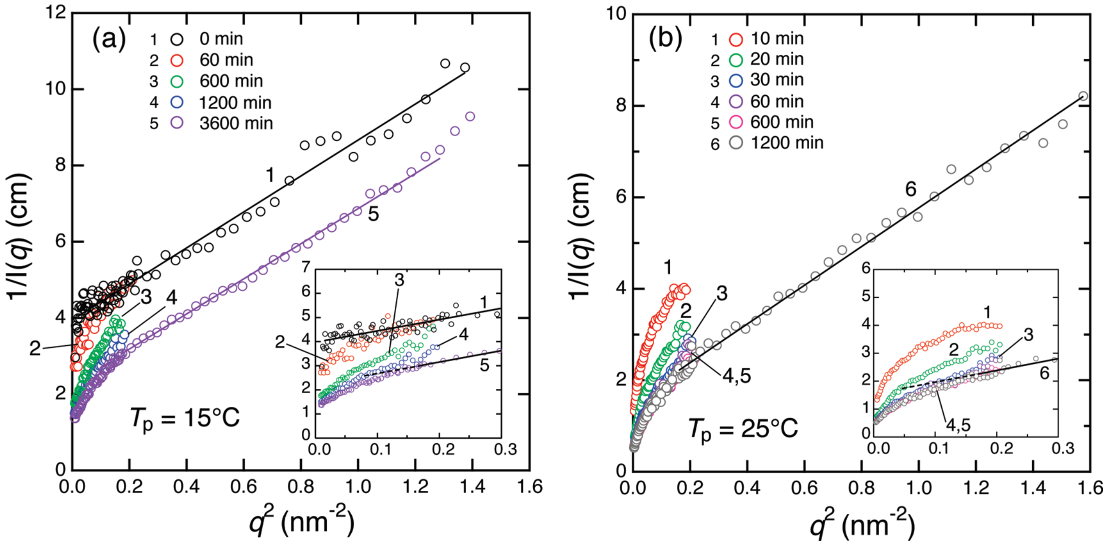

Figure 6. $1/I(q)$ plotted as a function of q^2 at (a) T_p = 15 °C and (b) T_p = 25 °C and the given polymerization times t. The solid lines are the best-fitted theoretical lines with the Ornstein−Zernicke equation. The lower q region of $0 \leq q^2$ (nm^{-2}) ≤ 0.3 is magnified in the inset.

smaller than that at $T_p \geq 34$ °C. The q-dependence of $I(q)$ are surely different from either the OZ behavior or the Porod-law behavior, which may indicate PNIPAAm block chains form a micelle core with an ill-defined interface, as evidenced by a lack of the q^{-4} law. The core is well swollen by water,[22] as evidenced by the decreased scattering intensity, compared with that at $T_p \geq 34$ °C, as a consequence of the fact that the difference in scattering length density between the micelle core and the surrounding medium is not so large as that at $T_p \geq 34$ °C. We believe that it is quite important to investigate quantitatively structure of this "soft-core" micelle. At T_p = 15 °C (Figure 5f), it is not clearly visible whether or not the scattering profiles during the reaction follow the OZ equation. If they obey the OZ equation, it turns out that the reaction occurs in the solution free from the soft micelles. Thus, it is crucial to critically check the scattering by means of the so-called OZ plot, $I(q)^{-1}$ versus q^2.

To quantitatively investigate the SANS profiles in detail at $15 \leq T_p$ (°C) ≤ 30, the OZ plots at T_p = 15 and 25 °C were conducted as shown in Figure 6a and b, respectively. At T_p = 15 °C (Figure 5f), the intensity of the time-resolved scattering profiles was generally weak, so that the statistical accuracy of the intensity data is relatively poor compared to that at $T_p \geq 25$ °C. Moreover, the measured time-resolved profiles are limited to the narrow q range so that the critical test of the OZ behavior is difficult. Consequently, we intended to put more weight on the data taken at steady states, either before (0 min) or after completion of the reaction (3600 min), than on the data taken during the reaction for the test of the OZ behavior. This is simply because the steady-state scattering profiles can be measured over wide enough q range and with the sufficient statistical accuracy. The result shown in Figure 6a shows the followings: (i) the profile before polymerization of NIPAAm (t = 0) (profile number 1) strictly obeys the OZ equation so that PEG exists in a homogeneous solution with thermal concentration fluctuations; (ii) the profile after the polymerization (profile number 5) exhibits a clear-cut deviation from the OZ behavior at $q^2 \leq 0.2$ nm^{-2}, elucidating that the solution during the polymerization (profile number 2 to 4) tends to exhibit the scattering profiles having a similar q dependence as that from the solution after the polymerization (profile number 5), though their intensity level increases with t. Thus, the solution during the polymerization also contains the soft-core micelles.

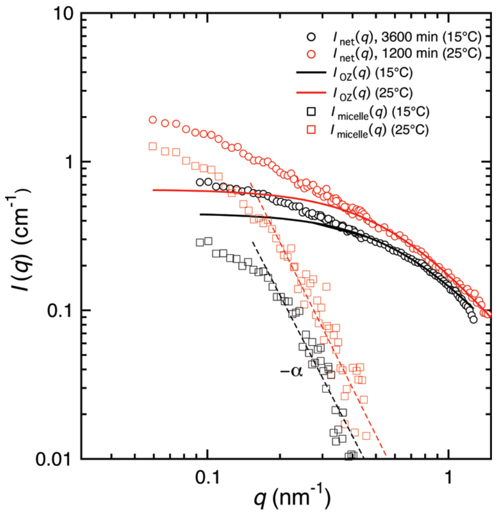

Figure 7. Decomposition of the net observed scattering (circles), $I_{net}(q)$, into the scattering from the thermal concentration fluctuations (solid lines), $I_{OZ}(q)$, and the soft-core swollen micelles in the solution (squares and broken lines), $I_{micelle}(q)$, obtained at T_p = 15 °C and t = 3600 min (black) and at T_p = 25 °C and t = 1200 min (red).

The exactly same argument can be applied to the solution at T_p = 25 °C. Consequently, it turns out that the soft-core micelles are formed during the whole polymerization time covered in this work in all the solutions at T_p(°C) = 15 and 25. The soft-core micelles cause the scattering excess at $q^2 \leq 0.2$ nm^{-2} from the OZ scattering, which is due to thermal concentration fluctuations of the bcp chains in the micelles and in the bulk solution and of unreacted PEG chains in the bulk solution. The excess scattering causes downward deviation from the linearity in the OZ plot. Thus, the net observed scattering, $I_{net}(q)$, is composed of two contributions: (i) one, $I_{OZ}(q)$, due to the thermal concentration fluctuations of bcp[33] and unreacted PEG and (ii) the other due to the soft-core micelles in the solution, $I_{micelle}(q)$. For the decomposition of the two contributions, we first estimated contribution (i) based on the OZ plot, that is, the linear relationship between $1/I(q)$ and q^2 (see the solid lines in Figure 6a), which determines the characteristic parameters $I(0)$ and ξ in $I_{OZ}(q)$ in eq 2. Then contribution (ii), denoted by $I_{micelle}(q)$, was obtained from $I_{net}(q) - I_{OZ}(q)$.

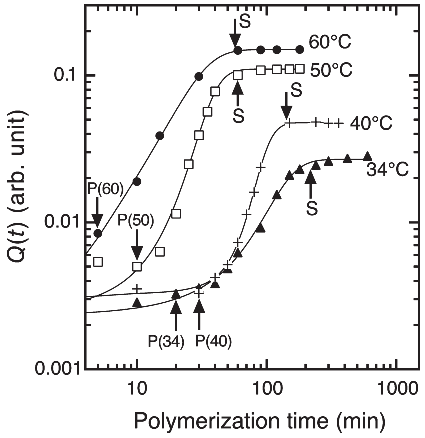

Figure 8. Integrated scattering intensity $Q(t)$ over the q range of $0.05 \leq q\ (\mathrm{nm}^{-1}) \leq 0.3$, plotted as a function of t at different T_p: 34 (triangles), 40 (crosses), 50 (squares), and 60 °C (diamonds). The solid lines are guides for eyes. $P(T_p)$ stands for the same meaning as in Figure 3. S stands for the saturation point in $Q(t)$ with t.

The obtained $I_{\mathrm{micelle}}(q)$ is presented as a function of q together with the $I_{\mathrm{net}}(q)$ and $I_{\mathrm{OZ}}(q)$ in Figure 7. $I_{\mathrm{micelle}}(q)$ was evaluated only for the profiles obtained after polymerization, because only these profiles allow the rigorous evaluation of $I_{\mathrm{OZ}}(q)$.

Thus, determined $I_{\mathrm{micelle}}(q)$ shown in Figure 7 tends to show the power-law behavior of $q^{-\alpha}$ at $q > 0.1\ \mathrm{nm}^{-1}$, where α is estimated to be 3.2 and 3.3 at 15 and 25 °C, respectively, though the corresponding q range is unfortunately wide enough for a rigorous determinations of α. If the $I_{\mathrm{micelle}}(q)$ is due to the surface fractal structure of the micelles, α is related to the surface fractal dimension, d_s, that is, $\alpha = 6 - d_s$,[48] so that $d_s = 2.8$ and 2.7 at 15 and 25 °C, respectively. The same analyses were conducted for the solution after the polymerization at $T_p = 30$ °C ($t = 600$ min). The results yield $d_s = 2.5$. Thus, it may be reasonable to consider that the interfaces of swollen micelles, formed after the polymerization at $15 \leq T_p\ (°\mathrm{C}) \leq 30$, are rather rough, the roughness tending to decrease with T_p. It may be well expected that the soft-core micelles formed during the polymerization also have similar rough surface.

To discuss the time evolution of the SANS $I(q)$ during the polymerization in a more quantitative manner, we evaluated the integral scattering intensity $Q(t)$ over the available range of q as a function of t

$$Q(t) = \int_{q_{\min}}^{q_{\max}} I(q,t)q^2 \mathrm{d}q \qquad (3)$$

The upper and lower limits for the integration, $q_{\min}$ and $q_{\max}$, are equal to 0.05 and 0.3 nm^{-1}, respectively. The integrated value $Q(t)$ thus evaluated reflects the structural changes occurring in the length scale from about 20 nm to about 100 nm and is roughly proportional to $\Delta B^2 \phi_{\mathrm{core}}(1 - \phi_{\mathrm{core}})$ as the solution forms the two-phase structure in which the micelle cores composed of PNIPAAm blocks are dispersed in the aqueous medium. Here, ϕ_{core} and ΔB^2 are the volume fraction of micelle cores and the scattering contrast between micelle cores and the matrix solution, respectively.

Figure 8 shows the time evolution of $Q(t)$ evaluated at T_p ranging from 34 to 60 °C. It is noted that both the $Q(t)$ and $C_M(t)$ start to increase at $t \approx 5$, 10, 30, and 20 min at $T_p = 60$, 50, 40, and 34 °C, respectively (also see Figure 3). These times correspond to those when the Porod law starts to be clearly discernible in the SANS profiles shown in Figure 5. (The SANS profiles at 40 °C are not included in Figure 5.) The specific points labeled with $P(T_p)$ in Figures 3, 4, and 8 designate the time beyond which the Porod law starts to be observed. Thus, the well-defined interface of the hard-core micelle is formed in the very early stage of the polymerization, as early as C_M being only 0.05 to 0.10. (The arrows marked by S will be described later in conjunction with Figure 9.)

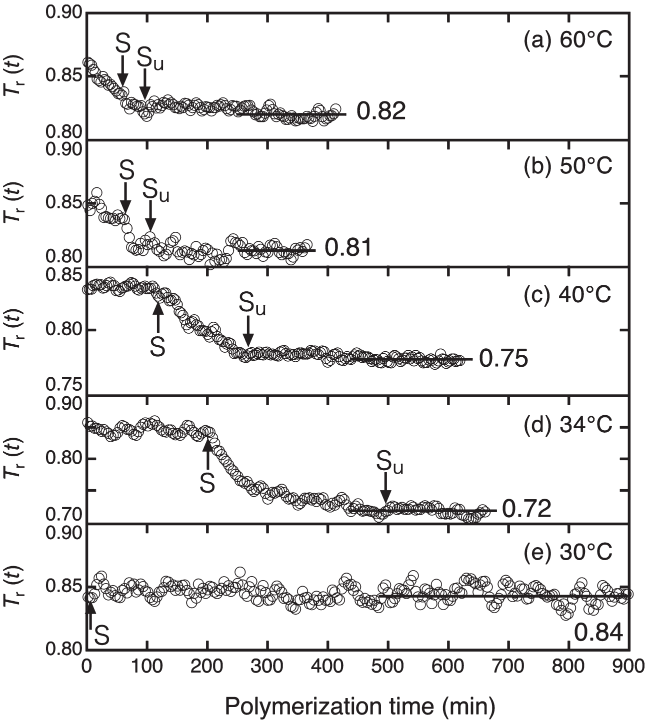

Figure 9. Time-resolved transmittance $T_r(t)$ obtained with the USANS spectrometer for the polymerization process at temperatures between 30 and 60 °C.

III-3. USANS and Transmittance Measurements. To investigate the micelle structure (micelle size and its spatial distribution), we need to investigate the scattering in a q range smaller than that covered by SANS. The Bonse-Hart (double crystal) type USANS spectrometer can approach the scattering in the low q range. USANS measurements, however, require extremely long measurement times (typically about 12 h) to cover a whole ultrasmall q range of 10^{-4} to $10^{-2}\ \mathrm{nm}^{-1}$, much longer than the characteristic time scales of the micelle formation during the polymerization. Therefore, the USANS measurements are limited to observation of the micelle structures after the completion of polymerization.

Prior to the USANS measurements, we performed time-resolved transmittance measurements, $T_r(t)$, which are expected to reflect the time evolution of the micelle formation during polymerization. $T_r(t)$ is defined by

$$T_r(t) \equiv I_t/I_0 = \exp(-\gamma_{\mathrm{total}} l) \qquad (4)$$

where I_0 and I_t are the incident neutron beam intensity before and after transmission of the reaction solution, respectively, l is the thickness of the solution along the incident beam direction, and γ_{total} is the total extinction coefficient of the solution. We can assume that γ_{total} is a sum of the following three kinds of extinction on incident neutron beam intensity: (i) absorption, γ_a, (ii) incoherent scattering, γ_{incoh}, and (iii) coherent scattering, γ_{coh}.

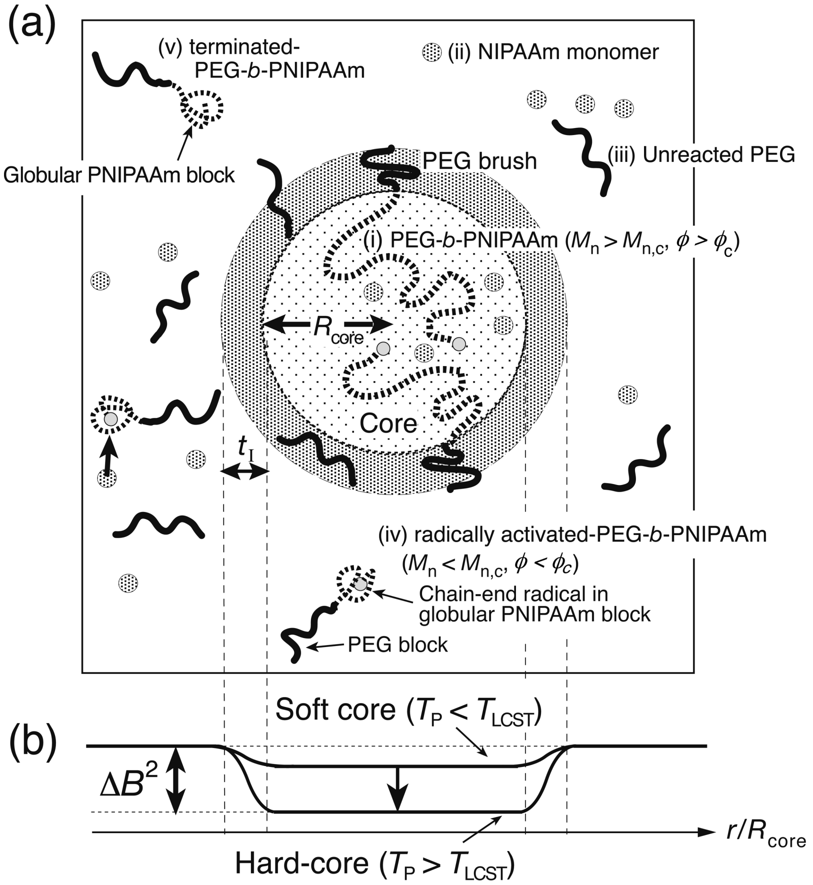

Figure 10. (a) Schematic illustration of the reaction field for the soap-free emulsion polymerization of PEG-*b*-PNIPAAm, which were polymerized from radically activated chain end of PEG. The polymerized PEG-*b*-PNIPAAm formed self-assembled micelles as a fundamental structure unit, when M_n and concentration ϕ_p of PNIPAAm block chain exceeds a critical molecular weight for the micelle formation $M_{n,c}$ and the critical concentration $\phi_{p,c}$. (b) Schematic diagram for a spatial distribution of the square of the scattering contrast ΔB for neutrons across the micelle in the medium of D_2O. At temperatures T_P above T_{LCST} of the aqueous solution of PNIPAAm (at around 31 °C), ΔB^2 dramatically becomes larger than that at $T_P < T_{LCST}$, because micelle cores composed of PNIPAAm block chain are strongly dehydrated. t_I is the characteristic interfacial thickness, which was estimated by the Porod analysis.

In Figure 9, $T_r(t)$ is plotted as a function of t. At all temperatures, $T_r(t = 0)$ is equal to about 0.85, which reflects the combined contributions of γ_a, γ_{incoh}, and $\gamma_{coh}(t = 0)$. Here, $\gamma_{coh}(t = 0)$ is attributed to the thermal concentration fluctuations of PEG, NIPAAm, and D_2O in the reaction solution before the polymerization. At T_p = 30 °C, $T_r(t)$ hardly changes with t from $T_r(t = 0)$, because the effect of extinction due to SANS from the micelle structure, $\gamma_{coh,micelle}$, on γ_{total} is relatively small compared to those of γ_a, γ_{incoh}, and $\gamma_{coh}(t = 0)$ on γ_{total}. Note that $I(q)$ at T_p = 30 °C is much smaller than $I(q)$ at T_p = 50 and 60 °C, as shown in Figure 5. At $T_p \geq 34$ °C, $T_r(t)$ decreases with t from $T_r(t = 0)$ to a value that depends on T_p. The decrease of $T_r(t)$ with t is due to the increasing contribution of the $\gamma_{coh,micelle}$ to γ_{total}. $T_r(t)$ at T_P = 34 °C, for example, decreases slightly with t up to 200 min (see the point marked by the arrow labeled by S) and then rapidly and largely decreases to a steady value of $T_r(\infty) = 0.72$ at $t > 500$ min (see the arrow labeled by S_u). The point S corresponds to time t_s when the increase of $Q(t)$ starts to saturate as shown in Figure 8, implying that $T_r(t)$ at T_p = 34 °C slightly decreases with t up to point S due to the increasing $\gamma_{coh,micelle}$. The further decrease of $T_r(t)$ beyond point S must reflect an additional increase of γ_{coh} with t, which we intuitively ascribe to increasing USANS intensity from the superstructure of the micelles, $\gamma_{coh,super}$. At T_p = 50 and 60 °C, point S shifts to a shorter time t, and $T_r(t)$ decreases to a lower value at point S compared with that at T_p = 34 °C. This fact well correlates with the fact that $Q(t)$ at T_p = 50 and 60 °C saturates at larger intensity levels and at shorter times than that at T_p = 34 °C. In contrast, $T_r(t)$ at 50 and 60 °C decreases only slightly beyond point S, which we intuitively ascribe to a smaller increase of $\gamma_{coh,super}$ at these temperatures than at T_p = 34 °C, as will be also confirmed later by the USANS profiles in Figure 12.

After $T_r(t)$ reaches the constant values, we performed USANS measurements. Figure 12 which will appear later in the text shows the combined USANS and SANS profiles at T_p ranging from 34 to 60 °C. The USANS measurements were conducted only at $T_p \geq 34$ °C as the USANS intensity level at $T_p \leq 30$ °C is rather weak compared with the intensity level of the background so that the USANS profiles cannot be accurately measured. We note that the combined USANS and SANS profile $I(q)$ at each T_p tends to show a crossover in the power law behavior of $I(q) \sim q^{-\alpha}$ at T_p-dependent crossover q, q_c. The higher the T_p, the larger is the q_c value. At $q < q_c$, the power-law exponent α depends on T_p, while at $q > q_c$, α is close to 4, irrespective of T_p.

It should be noted that the T_p-dependence of the USANS intensity is quite opposite to that of the SANS intensity, as shown in the inset of Figure 12; as T_p increases, the intensity of SANS increases, while that of USANS decreases. The large and slow decrease of $T_r(t)$ from point S down to point S_u at T_p = 34 °C (Figure 9d) should then be attributed to the

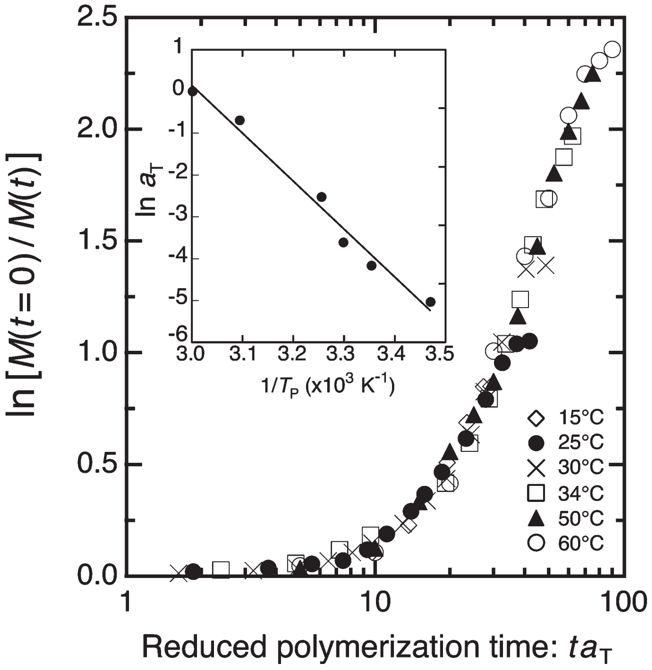

Figure 11. $\ln[M(t = 0)/M(t)]$ at various T_P ranging from 15 to 60 °C are plotted as a function of reduced polymerization time, $\ln(a_Tt)$. T_p dependence of the horizontal shift factor, a_T, is shown in the inset (Arrhenius plot), indicating that the slope of the solid line $(-\Delta H_a/R$, R = gas constant) is related to the activation energy of the addition reaction, ΔH_a (= 93.4 kJ/mol), between chain end radical and NIPAAm.

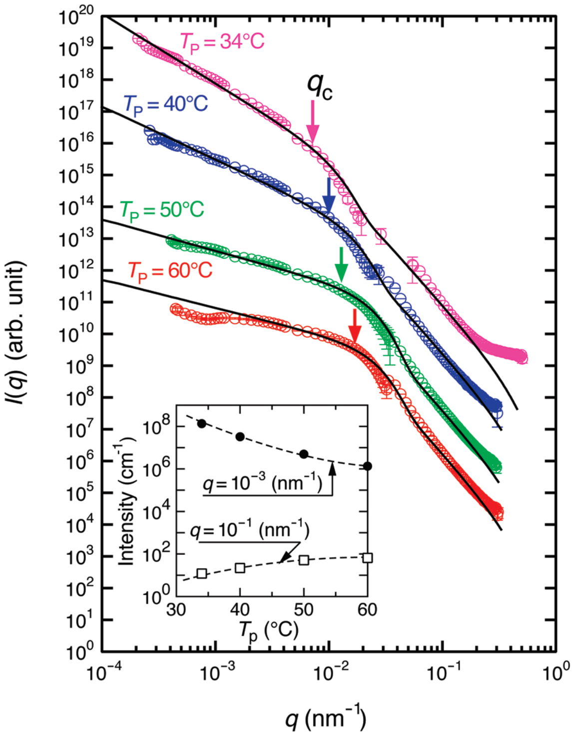

Figure 12. Combined ultrasmall- and small-angle neutron scattering intensity profile $I(q)$ obtained at different T_p: 34 (pink circles), 40 (blue circles), 50 (green circles), and 60 °C (red circles). Each profile was vertically shifted to avoid overlaps. The profiles at the q range of $q < 0.04$ (nm^{-1}) and $q \geq 0.03$ (nm^{-1}) were obtained by USANS and SANS spectrometers, respectively. The solid lines are the best-fitted theoretical profiles obtained by using eq 7 together with the characteristic parameters shown in Table 2. The scattering intensities at $q = 10^{-3}$ (nm^{-1}) (filled circles) and at $q = 10^{-1}$ (nm^{-1}) (open squares) are plotted as a function of T_p in the inset.

slow increase of the large USANS intensity and, hence, $\gamma_{\mathrm{coh,super}}$ with t. As T_p increases from 34 to 40 °C, the USANS intensity after the completion of polymerization becomes lower, which accounts for the increase of $T_r(\infty)$ from 0.72 to 0.75 and the small decrease of $T_r(t)$ from point S to S_u. Upon further increase of T_p to 50 or 60 °C, the USANS intensity decreases further, resulting in a further increase in $T_r(\infty)$. This accounts for the slight decrease of $T_r(t)$ beyond point S observed at T_p = 50 or 60 °C. Thus, the time evolution of $T_r(t)$ gives useful information on the time-evolution of the USANS profiles, which is difficult to directly measure at present time. We shall present a theoretical analysis of the combined USANS and SANS profiles on the basis of a unified approach[49,50] in section IV-4, which gives the best-fitted theoretical profiles shown by the solid lines in Figure 12.

IV. Discussion

IV-1. Background of the Soap-Free Emulsion Polymerization of PEG-*b*-PNIPAAm. Figure 10a schematically illustrates the concept of the soap-free emulsion polymerization of PEG-*b*-PNIPAAm at $T_p \geq 34$ °C (above lower critical solution temperature, T_{LCST}, of aqueous PNIPAAm solution), where the illustrated micelle shown in the center of Figure 10a is a fundamental structure unit, which builds up a higher-order structure (mass fractal structures in a larger length scale), as will be detailed later in the text (see section IV-4). When this radical polymerization of NIPAAm is carried out at $T_p \geq 34$ °C from the radically activated chain end of PEG, the propagating PNIPAAm block chains in PEG-*b*-PNIPAAm forms single-chain globules[23,25,26] [species (iv) and (v) in Figure 10a] . Because the globules are thermodynamically unstable in the solution, they aggregate themselves to form micelle cores stabilized by PEG brush chains emanating from the interface between the core and brush phases [as illustrated by species (i) in Figure 10a]. In the cores, which are substantially dehydrated at T_p > 32 °C, the PNIPAAm block chains are expected to be in a condensed phase swollen by NIPAAm monomer as a solvent. The block chains in the cores recover random coil conformations, which are more favorable than the globular conformations, and entangle obviously with other PNIPAAm block chains.

This micelle formation is brought about when the concentration of PNIPAAm block chains, ϕ_{PNIPAAm}, and M_n of the PNIPAAm block chains exceed a critical concentration, ϕ_c, and a critical molecular weight, $M_{n,c}$, in an aqueous matrix containing NIPAAm monomers [species (ii)], unreacted PEG [species (iii)], radically activated-bcps with $M_n < M_{n,c}$ [species (iv)], and terminated-bcps with $M_n < M_{n,c}$ [species (v)], as also shown in Figure 10a. Then, the PEG brush chains swollen by water and emanating from the interfaces of the cores acts as a stabilizer for the micelles. Thus, the polymerization under this condition may be conceptually treated as a "soap-free" emulsion polymerization and will provide a good model system to explore the necessary and sufficient condition for the quasi-living radical polymerization behaviors.

IV-2. Reaction Kinetics. Before going into detailed discussion on the reaction field for the quasi-living polymerization, it is useful to discuss further the temperature dependence of the reaction kinetics, as shown in Figures 3 and 4. It may be interesting to elucidate whether or not the specific reaction fields of the hard-core micelles (at $34 \leq T_p$ (°C) ≤ 60) and the soft-core micelles (at $15 \leq T_p$ (°C) ≤ 30) affect the reaction kinetics. $C_M(t)$ versus t at various T_ps in Figure 3 was replotted into $\ln[M(t = 0)/M(t)]$ versus t by using the relationship $M(t = 0)/M(t) = [1 - C_M(t)]^{-1}$, where $M(t = 0)$ and $M(t)$ are the monomer concentration at an initial state ($t = 0$) and at time t. If the reaction is the first order, we find

$$\ln[M(t = 0)/M(t)] = kt \qquad (5)$$

and, hence, the quantity $\ln[M(t = 0)/M(t)]$ should linearly increase with t, where the proportionality constant k is the reaction constant which depends on T_p. Furthermore, if the reaction mechanism is independent of T_p or the specific reaction fields, and if the reaction rate only depends on T_p, $\ln[M(t = 0)/M(t)]$ versus $\ln t$ at different T_ps should be superposed only by a horizontal shift with the shift factor $a_T \sim k$.

Figure 11 shows $\ln[M(t = 0)/M(t)]$ versus $\ln(a_T t)$, where the temperature dependence of the shift factor is shown in the inset. The kinetic data obtained at different T_ps superposed each other with respect to the reduced polymerization time $a_T t$ or kt. The result reveals itself that (i) the reaction mechanism is independent of the specific reaction fields (solution, soft-core micelle, or hard-core micelle; quasi-living-like field or non-living-like field) and that (ii) the reaction kinetics is not the first-order, and hence, eq 5 should be rewritten by

$$\ln[M(t = 0)/M(t)] = f(kt) \qquad (6)$$

where $f(kt)$ is the nonlinear universal function of $k(T_p)t$. Both results (i) and (ii) seem to be quite natural.

IV-3. Evidence for the Reaction Field for the Quasi-Living Polymerization. The time-resolved GPC results shown in Figure 4 clearly indicate that the soap-free emulsion polymerization at $T_p \geq 34$ °C proceeds living-likely with respect to each of the three criteria (i–iii) described in the beginning of section I. Criterion (ii) indicates suppression of the bimolecular termination reaction of chain-end radicals. The rate of increase of M_n with $C_M(t)$ decreases with increasing T_p at $T_p \geq 34$ °C, the relative slope of the $M_n(t)$ vs $C_M(t)$ plot at $T_p = 34$, 50, and 60 °C being 1, 0.7, and 0.6. This is at least partially due to a higher degree of suppression of bimolecular termination reactions and thus a larger number of propagating radicals at a higher T_p. Thus, M_n of PEG-*b*-PNIPAAm, synthesized at $T_p \geq 34$ °C, becomes smaller as T_p increases (see Table 1).

In situ and time-resolved SANS measurements in Figure 5 revealed that PEG-*b*-PNIPAAm forms self-assembled micelles in water during the polymerization at $T_p \geq 15$ °C when M_n and $\phi_{PNIPAAm}$ of the PNIPAAm chains exceed the critical values $M_{n,c}$ and ϕ_c. Thus, the polymerization takes place not only in the solution but also in the micelles at $t > t_c$, where t_c is the critical time for the micelle formation. The t_c varies with T_p: as T_p increases, t_c decreases.[51] The aqueous solution of PNIPAAm is known to have $T_{LCST} = 31$ °C.[23−27] Therefore, the water content in the micelle core, $\phi_{w,core}$, is expected to decrease drastically at $T_p \geq 34$ °C. Indeed, we found the following distinct differences between the SANS profiles at $T_p \geq 34$ °C and those at $15 \leq T_p$ (°C) ≤ 30: at $T_p \geq 34$ °C, the SANS profiles show the q-dependence close to q^{-4} (the Porod law),[47] relevant to the well-defined interface of the PNIPAAm micelle core, whereas at $15 \leq T_p$ (°C) ≤ 30, SANS is weak and does not show the Porod law, suggesting swollen micelle cores with ill-defined interfaces (see Figure 7, for example). Figure 10b schematically illustrates the spatial distribution of the square of the scattering contrast ΔB^2 across the micelle. The dehydration of the core is more pronounced as the T_p increases. Hence, ΔB^2 increases with T_p. This is why we observe a drastic change in SANS intensity between $T_p \leq 30$ °C and $T_p \geq 34$ °C; the scattering intensity at $q \sim 0.03$ nm^{-1} at $T_p = 60$ °C is on the order of 10^4 cm^{-1}, whereas that at $T_p = 30$ °C is on the order of 10^1 cm^{-1}, as shown in Figure 5a,d. On the basis of these findings, the quasi-living behaviors of the soap-free emulsion polymerization should be related to the $\phi_{w,core}$.

It is important to note that the scattering profile $I(q)$, which satisfies the Porod law, can be observed at the early stage of polymerization at $T_p \geq 34$ °C, that is, $t \sim 20$ min at $T_p = 34$ °C, $t \sim 10$ min at $T_p = 50$ °C, and $t \sim 5$ min at $T_p = 60$ °C, as shown in Figure 5. The C_Ms attained at these times are as low as 0.05−0.1, as marked with P(T_p) labeled arrows in Figures 3 and 4a, which indicates that at these T_ps the dehydrated micelle cores (hard cores) composed of propagating PNIPAAm block chains, and thus the reaction fields for the quasi-living soap-free emulsion polymerization are formed in the very early stage of the polymerization. In principle, the chain-end radicals encounter two kinds of reaction field, that is, (i) a more or less homogeneous solution at $t < t_c$ and (ii) a hard core at $t \geq t_c$. The chain-end radicals spend only a minor fraction of their lifetime in the former reaction field at high T_p, which is the primary reason for the quasi-living polymerization behaviors.

Let us discuss here effects of the initiation of the radicals via the oxidation reaction between Ce$^{(IV)}$ and PEG on the quasi-living polymerization behaviors described above. Feijen and co-workers reported the fact that [Ce$^{(IV)}$] and [unreacted-PEG] exhibits sharp decrease immediately after the start of polymerization within $t = 5$ min at $T_p = 60$ °C.[15] This result indicates that the generation of radicals completed in the very early stage of polymerization, whereas, in the conventional emulsion polymerizations with normal initiators, for example, AIBN and BPO, the radicals gradually generate during the course of polymerization. However, even in this special initiation process with Ce$^{(IV)}$, the propagating radicals in the solution can still undergo the recombination reaction for the termination. Hence, in this sense the catalytic effect itself is not the sufficient condition for the quasi-living polymerization mechanism.

We have already pointed out in section III-2 that at $15 \leq T_p$ (°C) ≤ 30 soft micelles are formed also at a very early stage of the polymerization, that is, $t \sim 60$ min at $T_p = 15$ °C, $t \sim 10$ min at $T_p = 25$ °C, and $t \sim 20$ min at 30 °C (Figures 5f−d) or at C_M as small as 0.05 in all the cases. The swollen micelle core, however, does not satisfy the criteria of the reaction field for the quasi-living polymerization.

IV-4. Theoretical Analysis of Combined USANS and SANS Intensity Distribution. We define the radius of gyration of the micelle core, $R_{g,core}$, as a fundamental building unit comprising the superstructure or higher-order structures responsible for the combined USANS and SANS profiles shown by the symbols (circles) in Figure 12. If the core is described by a sphere of radius R_{core}, then $R_{g,core}^2 = (3/5)R_{core}^2$. Because the shape of the micelle core is not necessarily spherical, we describe the core in terms of $R_{g,core}$.

We carried out a theoretical analysis of the combined profile in the context of the unified Guinier and power-law approach[49,50]

$$I(q) = Aq^{-\alpha}\exp(-q^2R_{g,core}^2/3) + B\exp(-q^2R_{g,core}^2/3) + C\left[q^{-1}erf(-qR_{g,core}/\sqrt{6})\right]^{\beta}\exp(-\sigma_I{}^2q^2) \qquad (7)$$

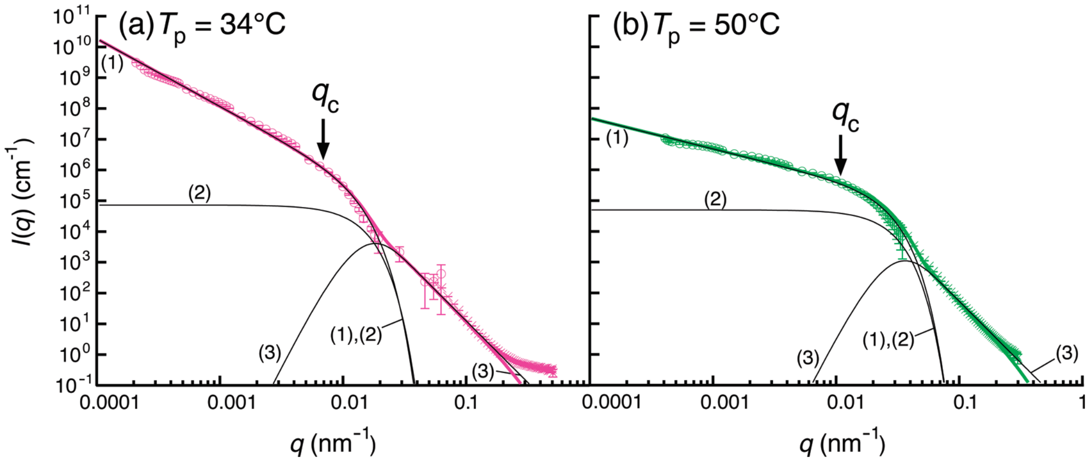

Figure 13. Combined ultrasmall- and small-angle neutron scattering intensity profile $I(q)$ obtained at (a) T_p = 34 °C and (b) T_p = 50 °C after the completion of the polymerization (colored symbols). The colored solid line is the best-fitted theoretical scattering profile, using eq 7, which is a sum of the three solid lines numbered 1−3, representing the first term to the third term in the rhs of eq 7, respectively.

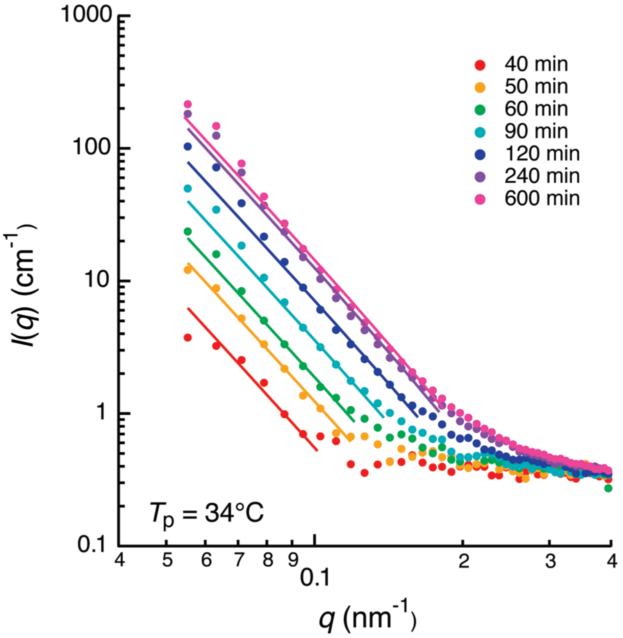

Figure 14. Small-angle neutron scattering profiles highlighted at the q range sensitive to the interface of the core micelle at T_p = 34 °C and the given t. The solid lines are the best-fitted theoretical profiles based on eq 9 with experimental profiles (symbols).

The power-law behavior of $q^{-\alpha}$ observed in the q range of q (nm^{-1}) < 0.01 can be described by the first term of the right-hand side (rhs) of eq 7, where the term $\exp(-q^2R_{g,\,core}^2/3)$ serves as a damping factor for the power law at the large q limit, and $R_{g,core}$ or $q_c = 1/R_{g,core}$ (indicated by arrows in Figure 12) specifies the lower cutoff length or the upper cutoff wavenumber for the power law.

The second term on the rhs of eq 7 describes the scattering from the building unit of the superstructure or the mass fractal structure, while the third term describes the power law behavior in the q range of q (nm^{-1}) > 0.05 with $\beta \cong 4$, and the term $[erf(-qR_{g,\,core}/\sqrt{6})]^{\beta}$ describes the damping factor for the power law of $q^{-\beta}$ at the lower q limit where $R_{g,core}$ and $q_c = 1/R_{g,core}$ are, respectively, the upper cutoff length and the lower cutoff wavenumber for the power law of $q^{-\beta}$. In this analysis, we set $\beta = 4$ and incorporated the term $\exp(-\sigma_I{}^2q^2)$ describing the diffuse interface boundary, where σ_I is the parameter characterizing the interfacial thickness. A, B, and C are the proportionality constants describing the relative contributions of these three terms to the net scattering intensity $I(q)$. In this work we assume that polydispersity in $R_{g,core}$ can be neglected for simplicity and as a first step of the analysis.

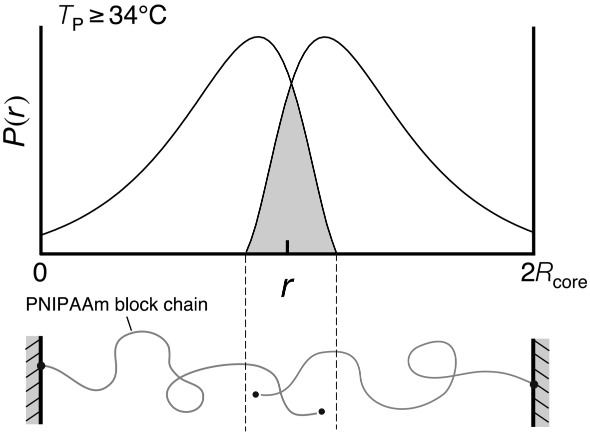

Figure 15. Statistical mechanical interpretation of the so-called "compartmentalization" of the chain-end radicals in the micelle cores at $T_p \geq 34$ °C.

It should be noted in Figure 12 that the best-fitted theoretical profiles (solid lines) well reproduce the experimentally observed combined small-angle scattering (circular symbols) except for a small deviation from the observed profiles at the large q-limit. This small deviation is quite obviously attributed to the effect of thermal concentration fluctuations, which naturally exists in the real system. The deviation evidently becomes larger as T_p decreases because the micelle cores tend to be swollen more by water and a larger amount of the block copolymers tend to exist in the solution with increasing T_p.

The solid black lines in Figure 12 show the theoretical scattering curves best-fitted with the experimental ones (colored symbols). Figure 13 demonstrates the contribution of each term in the rhs of eq 7 to the best-fitted theoretical scattering curve for the combined USANS and SANS profiles at T_p = (a) 34 °C and (b) 50 °C. The decomposed lines, numbered (1) to (3), represent the contribution of the first term to the third term in the rhs of eq 7 to the net scattering intensity $I(q)$ (the colored solid line). The characteristic parameters $R_{g,core}$, α, and β obtained by best-fitting are

Table 2. Summary of Characteristic Parameters Determined by the In Situ SANS and USANS Experiments after the Completion of the Polymerization at Varying T_p

T_p	34	40	50	60
$R_{g,core}$ (nm)	142	97	69	62
$q_c \times 10^2$ (nm^{-1})	0.70	1.03	1.44	1.61
α	2.23	1.68	1.07	1.02
β	4	4	4	4
t_I (nm)	6.7	6.4	6.1	6.1

summarized in Table 2. As T_p increases, both $R_{g,core}$ and α tend to decrease, implying that (i) the size of the fundamental structure unit, which builds up the superstructures, becomes small and that (ii) the superstructures tend to have a mass-fractal structure with a smaller mass-fractal dimension.

The size of the fundamental structure unit is much larger than that expected for the spherical domains composed of PNIPAAm block chains in PEG-*b*-PNIPAAm melt having $M_n = (11.6-7.0) \times 10^4$: The expected R_{core} calculated by the Helfand and Wasserman theory[52] is about 50 nm (see Figure 10 of ref 52). Thus, the fundamental structure unit at T_p = 60 °C might be composed of aggregated spherical domains of $N \cong (\sqrt{5/3}R_{g,core}/50)^3 = 4.1$. The aggregation may be plausible in light of the large block ratio of PNIPAAm to PEG shown in Table 1, which indicates that relatively short PEG brushes emanate from a large core. This may cause an insufficient coverage of the interfacial area of the micelle core by PEG brushes, which in turn causes the entropic repulsion between the spherical domains small, allowing the aggregation to occur to a certain extent. The characteristic interfacial thickness t_I[53,54] in Table 2 is related to the parameter σ_I by

$$t_I = \sqrt{2\pi}\sigma_I \tag{8}$$

At the large q-limit, where the scattering is sensitive to the interface of the micelle cores, $I(q)$ in eq 7 is given by

$$I(q) \sim q^{-4} \exp(-\sigma_I{}^2 q^2) \tag{9}$$

According to eq 9, the parameter σ_I is determined from the Porod plot, $\ln[I(q)q^4]$ versus q^2.[53,55,56] Figure 14 highlights the scattering profile focused on the q range sensitive to the interface. The solid lines show the best fit of the experimental scattering profiles with the theoretical scattering profiles given by eq 9, with the parameter σ_I being determined by the Porod plot and shown in Table 2. The deviation of the experimental profiles from the solid lines at the large q range is attributable to the contribution of the thermal concentration fluctuations.

IV-5. Origin for the Quasi-Living Polymerization Behavior. Once the radically active PNIPAAm chain ends are confined in the solid-like micelle cores, the polymerization rate may slow down, because the NIPAAm monomer diffuses more slowly in the core than in the water matrix and because the living chain ends also diffuse more slowly in the core. The slowly propagating PNIPAAm block chains in the cores, which have been formed earlier in the water and already confined in the core, are caught up by the propagating PNIPAAm block chains formed later in the water.

To bring about the quasi-living polymerization behavior, the low diffusivity of PNIPAAm chain ends in the solid-like core above T_p = 34 °C is crucial, as already pointed out. Besides the reduced mobility of the chain-end radicals in the micelle cores, we should also take into account the temperature dependence of the probability of the two chain ends to come into contact in the micelle core. Figure 15 shows a schematic illustration of the probability distribution function $P(r)$ of the chain ends of PNIPAAm block chains emanating from the interface of the micelle core having the radius R_{core}.

At $T_p \geq 34$ °C, the chain-end radicals of PNIPAAm may be localized, or so-called "compartmentalized", in the central region of solid-like cores of micelles,[57−59] as schematically shown in Figure 15. The localization of the chain ends effectively suppress the probability of two chain-ends of PNIPAAm block chains emanating from the opposite side of the interface to encounter each other. This may appear to be against our intuition at a first glance, but it turns out to be reasonable: the probability is proportional to (i) the area of the hatched gray region, where the two functions $P(r)$ with their origins at $r = 0$ and at $r = 2R_{core}$ overlap, and to (ii) the number of the cores. Both factors (i) and (ii) decrease with increasing $\chi_{AB}N$. More specifically, the factor (i) goes to zero as $\chi_{AB}N \rightarrow \infty$. This effect in turn suppresses the bimolecular termination reactions and, hence, brings about the quasi-living polymerization behavior. At $15 \leq T_p$ (°C) ≤ 30, on the other hand, the micelle cores are swollen with water and the effective segregation power $\chi_{AB}N$ between PEG and PNIPAAm block chains is weaker than that at $T_p \geq 34$ °C. Hence, the distribution function of the chain ends $P(r)$ is much broader than $P(r)$ at $T_p \geq 34$ °C, giving rise to a larger overlap area, which makes factors (i) and (ii) become larger and leads to "decompartmentalization".

V. Conclusion

We investigated a soap-free emulsion polymerization to synthesize a poly(*N*-isopropylacrylamide) (PNIPAAm) block chain in poly(ethylene glycol)-*block*-poly(*N*-isopropylacrylamide) (PEG-*b*-PNIPAAm) starting from the radically activated chain end of poly(ethylene glycol) (PEG). We like to stress that the time-resolved SANS gave a strong impact to clarify the important key question of when the specific reaction field required for soap-free emulsion polymerization is created in the reaction system via the reaction-induced self-assembly. The SANS straightforwardly elucidated that the reaction field, either the soft-core micelle or the hard-core micelle, is self-assembled from the very early stage of the polymerization, where the monomer conversion $C_M(t)$ reaches about 0.05, until the end of the polymerization. The reaction field responsible for the quasi-living polymerization is the one given by the solid-like cores of PNIPAAm blocks, which entrap the chain-end radicals in such a way that one end of the PNIPAAm block chains is confined at the core interface and the other end carrying the active chain-end radical is confined around the center of the domains, while the whole PNIPAAm block chain is confined in the core. The entrapment brings about (i) the low diffusivity of the chain-end radicals (**a dynamical effect**) and (ii) the effective suppression of the two chain-end radicals to encounter each other (**a static effect**), both of which suppress the bimolecular termination reactions. The entrapment causing the above two effects is believed to account for a physical interpretation of the so-called "compartmentalization".

Our work may suggest that almost any emulsion polymerization at high conversion would have restricted mobility and would therefore be quasi-living like. In this regard, however, we cannot forget the fact that the polymerization in this case cannot be quasi-living before achieving the high conversion and the restricted mobility. Moreover, the entrapment or the compartmentalization discussed above is responsible for a more severe restricted motion than the restricted motion encountered by the conventional emulsion polymerization at high conversions. It may also be important to note that the specific reaction field built up for the quasi-living polymerization is primarily brought about by the physical factors rather than the specific catalytic effect, as we briefly described in the paragraph preceding the last paragraph in section IV-3. The physical factors build up the specific reaction field from the very low conversion.

Finally we would like to note that the time-resolved SANS will provide some more rich information other than the key information discussed here in this paper, such as the core size, association number of the block chains in the core as a function of polymerization time, and so on. Such quantitative studies as described above deserves future work.

Acknowledgment. The authors would like to gratefully acknowledge Prof. Toshihiro Kawakatsu for interest and enlightening discussion and Mr. Fumiya Nakata and Mr. Tsutomu Ishimaru of TOSOH Co. Ltd. for technical support and helpful discussions on GPC.

References and Notes

(1) Motokawa, R.; Nakahira, T.; Annaka, M.; Hashimoto, T.; Koizumi, S. *Polymer* **2004**, *45*, 9019–9022.
(2) Topp, M. D. C.; Dijkstra, P. J.; Talsma, H.; Feijen, J. *Macromolecules* **1997**, *30*, 8518–8520.
(3) Matyjaszewski, K.; Patten, T. E.; Xia, J. *J. Am. Chem. Soc.* **1997**, *119*, 674–680.
(4) Kamigaito, M.; Ando, T.; Sawamoto, M. *Chem. Rev.* **2001**, *101*, 3689–3746.
(5) Chiefari, J.; Chong, Y. K.; Ercole, F.; Krstina, J.; Jeffery, J.; Le, T. P. T.; Mayadunne, R. T. A.; Meijs, G. F.; Moad, C. L.; Moad, G.; Rizzardo, E.; Thang, S. H. *Macromolecules* **1998**, *31*, 5559–5562.
(6) Hawker, C. J.; Bosman, A. W.; Harth, E. *Chem. Rev.* **2001**, *101*, 3661–3688.
(7) Harkins, W. D. *J. Chem. Phys.* **1945**, *13*, 381–382.
(8) Harkins, W. D. *J. Chem. Phys.* **1946**, *14*, 47–48.
(9) Harkins, W. D. *J. Am. Chem. Soc.* **1947**, *69*, 1428–1444.
(10) Smith, W. V.; Ewart, R. H. *J. Chem. Phys.* **1948**, *16*, 592–599.
(11) Fitch, R. M. *Polymer Colloids, A Comprehensive Introduction*; Academic Press: New York, 1997.
(12) Parker, H.-Y.; Westmoreland, D. G.; Chang, H.-R. *Macromolecules* **1996**, *29*, 5119–5127.
(13) Fitzwater, S.; Chang, H. R.; Parker, H. Y.; Westmoreland, D. G. *Macromolecules* **1999**, *32*, 3183–3189.
(14) Sato, T.; Otsu, T. *Adv. Polym. Sci.* **1985**, *71*, 41–77.
(15) Topp, M. D. C.; Leunen, I. H.; Dijkstra, P. J.; Tauer, K.; Schellenberg, C.; Feijen, J. *Macromolecules* **2000**, *33*, 4986–4988.
(16) Han, C. D.; Vaidya, N. Y.; Kim, D.; Shin, G.; Yamaguchi, D.; Hashimoto, T. *Macromolecules* **2000**, *33*, 3767–3780.
(17) Dormidontova, E. E.; Lodge, T. P. *Macromolecules* **2001**, *34*, 9143–9155.
(18) Bates, F. S.; Fredrickson, G. H. *Annu. Rev. Phys. Chem.* **1990**, *41*, 525–557.
(19) Hashimoto, T. In *Thermoplastic Elastomers*, 3rd ed.; Holden, G., Kicheldorf, H. R., Quirk, R. P., Eds.; Hanser: Munich, Germany, 2004; Chap. 18, pp 457−491.
(20) Hamley, I. W. *The Physics of Block Copolymers*; Oxford University Press: New York, 1998.
(21) Hasegawa, H. Hashimoto, T. In *Comprehensive polymer science*; Aggarwal, S. L., Russo, S., Eds.; Pergamon Press: New York, 1996; Chap. 14, pp 497−539.
(22) Motokawa, R.; Koizumi, S.; Annaka, M.; Nakahira, T.; Hashimoto, T. *Prog. Colloid Polym. Sci.* **2005**, *130*, 85–96.
(23) Fujishige, S.; Kubota, K.; Ando, I. *J. Phys. Chem.* **1989**, *93*, 3311–3313.
(24) Schild, H. G.; Tirrell, D. A. *J. Phys. Chem.* **1990**, *94*, 4352–4356.
(25) Wang, X.; Qiu, X.; Wu, C. *Macromolecules* **1998**, *31*, 2972–2976.
(26) Wang, X.; Wu, C. *Macromolecules* **1999**, *32*, 4299–4301.
(27) Kujawa, P.; Winnik, F. M. *Macromolecules* **2001**, *34*, 4130–4135.
(28) Motokawa, R.; Annaka, M.; Nakahira, T.; Koizumi, S. *Colloids Surf., B* **2004**, *38*, 213–219.
(29) Motokawa, R.; Morishita, K.; Koizumi, S.; Nakahira, T.; Annaka, M. *Macromolecules* **2005**, *38*, 5748–5760.
(30) Helfand, E.; Tagami, Y. *J. Chem. Phys.* **1972**, *56*, 3592–3601.
(31) Hashimoto, T.; Shibayama, M.; Kawai, H. *Macromolecules* **1983**, *16*, 1093–1101.
(32) Hashimoto, T.; Mori, K. *Macromolecules* **1990**, *23*, 5347–5351.
(33) It should be noted that the OZ scattering itself reveals that the thermal concentration fluctuation between the solvent and the bcp dominates the thermal concentration fluctuations between PNIPAAm and PEG blocks. Otherwise, the scattering showed a scattering maximum arising from the correlation hole effect.[46] This is reasonable in light of the fact that the difference in the scattering length between PEG and PNIPAAm is much smaller than that between PEG and D_2O and that between PNIPAAm and D_2O.
(34) Table 3 and Figure 7a in ref 22 suggest that a crossover from the soft-core micelles to the hard-core micelles occurs in the PEG-*b*-PNIPAAm aqueous solution in the narrow temperature range between 31 and 32 °C. This temperature is slightly higher than $T_{\mathrm{LCST}} = 31$ °C for aqueous solutions of PNIPAAm homopolymer. It should be noted that there were typos in the figure legend in Figure 7a in ref 22 where the temperatures from 30 to 34 °C indicated in the plots should be read as 31 to 35 °C, respectively.
(35) Ganachaud, F.; Monterio, M. J.; Gilbert, R. G.; Dourges, M. A.; Thang, S. H.; Rizzardo, E. *Macromolecules* **2000**, *33*, 6738–6745.
(36) Koizumi, S.; Iwase, H.; Suzuki, J.; Oku, T.; Motokawa, R.; Sasao, H.; Tanaka, H.; Yamaguchi, D.; Shimizu, H. M.; Hashimoto, T. *Phys. B* **2006**, *385−386*, 1000–1006.
(37) Koizumi, S.; Iwase, H.; Suzuki, J.; Oku, T.; Motokawa, R.; Sasao, H.; Tanaka, H.; Yamaguchi, D.; Shimizu, H. M.; Hashimoto, T. *J. Appl. Crystallogr.* **2007**, *40*, s474–s479.
(38) Bonse, U.; Hart, M. *Appl. Phys. Lett.* **1968**, *7*, 238–240.
(39) Aizawa, K; Tomimitsu, H. *Phys. B* **1995**, *213-214*, 884–886.
(40) Yamaguchi, D.; Koizimi, S.; Motokawa, R.; Kumada, T.; Aizawa, K.; Hashimoto, T. *Phys. B* **2006**, *385−386*, 1190–1193.
(41) Glatter, O.; Kratky, O. *Small Angle X-ray Scattering*; Academic Press: London, 1982.
(42) Ray, B.; Isobe, Y.; Morioka, K.; Habaue, S.; Okamoto, Y.; Kamigaito, M.; Sawamoto, M. *Macromolecules* **2003**, *36*, 543–545.
(43) Ray, B.; Isobe, Y.; Matsumoto, K.; Habaue, S.; Okamoto, Y.; Kamigaito, M.; Sawamoto, M. *Macromolecules* **2004**, *37*, 1702–1710.
(44) Zhang, W.; Shi, L.; Wu, K.; An, Y. *Macromolecules* **2005**, *38*, 5743–5747.
(45) Ornstein, L. S.; Zernicke, F. *Proc. Akad. Sci.* **1914**, *14*, 793–806.
(46) deGennes, P. G. *Scaling Concepts in Polymer Physics*; Cornell University Press: Ithaca, NY, 1979.
(47) Porod, G. *Kolloid-Z.* **1951**, *124*, 83−114; **1952**, *125*, 51−57, 108−122.
(48) Higgins, J. S.; Benoît, H. C. *Polymers and Neutron Scattering*; Oxford University Press: Oxford, 1994.
(49) Beaucage, G. *J. Appl. Crystallogr.* **1995**, *28*, 717–728.
(50) Beaucage, G.; Kammler, H. K.; Pratsinis, S. E. *J. Appl. Crystallogr.* **2004**, *37*, 523–535.
(51) Qualitative examination of the changes in the scattering profiles with time shown in Figure 5 together with quantitative examination of those shown in Figures 6 and 7 indicate that the t_c values are shorter than 5, 10, 20, 20, 10, and 60 min at T_p = 60, 50, 34, 30, 25, and 15 °C, respectively. These t_c values are indicated by the arrows marked with P(T_p) in Figures 3, 4, and 8, where T_p, in this case, too, indicates the polymerization temperature. These t_c values shown by P(T_p)s in Figure 3 reveal $C_M(t_c) \le 0.05$, independent of T_p, which in turn elucidates $\phi(t_c) \le 3.4 \times 10^{-3}$ and $M_n(t_c) \le 1.0 \times 10^4$ at $34 \le T_p$ (°C) ≤ 60.
(52) Helfand, E.; Wasserman, Z. R. *Macromolecules* **1978**, *11*, 960–966.
(53) Hashimoto, T.; Fujimura, M.; Kawai, H. *Macromolecules* **1980**, *13*, 1660–1669.
(54) Hashimoto, T.; Shibayama, M; Kawai, H. *Macromolecules* **1980**, *13*, 1237–1247.
(55) Ruland, W. *J. Appl. Crystallogr.* **1971**, *4*, 70–73.
(56) Shibayama, M.; Hashimoto, T. *Macromolecules* **1986**, *19*, 740–749.
(57) Milner, S. T.; Witten, T. A.; Cates, M. E. *Macromolecules* **1988**, *21*, 2610–2619.
(58) Kawasaki, K.; Kawakatsu, T. *Macromolecules* **1990**, *23*, 4006–4019.
(59) Torikai, N.; Noda, I.; Karim, A.; Satija, S. K.; Han, C. C.; Matsushita, Y.; Kawakatsu, T. *Macromolecules* **1997**, *30*, 2907–2914.